Single and dual energy attenuation correction in PET/CT in the presence of iodine based contrast agents

Niklas S. Rehfeld[a)]
Laboratory for Preclinical Imaging and Imaging Technology of the Werner Siemens-Foundation, University of Tübingen, Röntgenweg 13, D-72076, Tübingen, Germany; Nuclear Medicine, Department of Radiology, University of Tübingen, Otfried-Müller-Straße 14, D-72076 Tübingen, Germany and Diagnostic Radiology, Department of Radiology, University of Tübingen, Hoppe-Seyler-Straße 3, D-72076 Tübingen, Germany

Björn J. Heismann
Siemens AG Medical Solutions, Siemensstr. 1, D-91301 Forchheim, Germany

Jürgen Kupferschläger
Nuclear Medicine, Department of Radiology, University of Tübingen, Otfried-Müller-Straße 14, D-72076 Tübingen, Germany

Philip Aschoff
Diagnostic Radiology, Department of Radiology, University of Tübingen, Hoppe-Seyler-Straße 3, D-72076 Tübingen, Germany

Gunter Christ
Department of Radio-oncology, University of Tübingen, Hoppe-Seyler-Straße 3, D-72076 Tübingen, Germany

Anna C. Pfannenberg
Diagnostic Radiology, Department of Radiology, University of Tübingen, Hoppe-Seyler-Straße 3, D-72076 Tübingen, Germany

Bernd J. Pichler
Laboratory for Preclinical Imaging and Imaging Technology of the Werner Siemens-Foundation, University of Tübingen, Röntgenweg 13, D-Tübingen, Germany, D-72076, Tübingen, Germany

(Received 4 December 2007; revised 7 March 2008; accepted for publication 7 March 2008; published 24 April 2008)

In present positron emission tomography (PET)/computed tomography (CT) scanners, PET attenuation correction is performed by relying on the information given by a single CT scan. The scaling of the linear attenuation coefficients from CT x-ray energy to PET 511 keV gamma energy is prone to errors especially in the presence of CT contrast agents. Attenuation correction based upon two CT scans at different energies but performed at the same time and patient position should reduce such errors and therefore improve the accuracy of the reconstructed PET images at the cost of introduced additional noise. Such CT scans could be provided by future PET/CT scanners that have either dual source CT or energy sensitive CT. Three different dual energy scaling methods for attenuation correction are introduced and assessed by measurements with a modified NEMA 1994 phantom with different CT contrast agent concentrations. The scaling is achieved by differentiating between (1) Compton and photoelectric effect, (2) atomic number and density, or (3) water-bone and water-iodine scaling schemes. The scaling method (3) is called hybrid dual energy computed tomography attenuation correction (hybrid DECTAC). All three dual energy scaling methods lead to a reduction of contrast agent artifacts with respect to single energy scaling. The hybrid DECTAC method resulted in PET images with the weakest artifacts. Both, the hybrid DECTAC and Compton/photoelectric effect scaling resulted also in images with the lowest PET background variability. Atomic number/density scaling and Compton/photoelectric effect scaling had problems to correctly scale water, hybrid DECTAC scaling and single energy scaling to correctly scale Teflon. Atomic number/density scaling and hybrid DECTAC could be generalized to reduce these problems. © *2008 American Association of Physicists in Medicine*. [DOI: 10.1118/1.2903476]

Key words: dual energy scaling of linear attenuation coefficients, PET/CT

I. INTRODUCTION

The additional morphological information provided by positron emission tomography/computed tomography (PET/CT) scanners[1] in contrast to stand alone PET scanners can be of additional diagnostic value for the physician.[2] Another benefit of PET/CT systems is the faster examination time, since the attenuation map to correct PET data is obtained from the CT scan and not from the much longer transmission scan.[3,4] The benefits of the combined scanner are opposed by several PET image artifacts that are caused by the CT-based attenu-

ation correction: CT field of view (FOV) truncation artifacts, beam hardening artifacts, motion (heartbeat, respiration, movement) artifacts, and artifacts caused by the scaling of linear attenuation coefficients from CT photon energy (around 50–80 keV mean energy) to linear attenuation coefficients at 511 keV.[1,5–8] We hypothesize that, with the exception of truncation and movement, all mentioned artifacts could be reduced, if attenuation correction was based upon two sets of CT data that were measured using x-ray photons of different energy.

At present, this information can be obtained by two consecutive scans with different peak energies. However, since the two scans are not performed at the same time and due to patient movement, the images are not exactly congruent and the resulting dual energy attenuation correction is erroneous. The magnitude of this error depends on the PET resolution, the magnitude of patient movement, and (if present) the quality of the CT/CT registration of the two CT scans.

Simultaneous scans reducing such errors could be performed if the CT component of a PET/CT scanner was replaced by a dual source or energy sensitive CT. Present dual source CT scanners contain one source of limited transaxial field of view and therefore provide dual energy images of the central part of the images, whereas in the outer regions only information of a single energy scan is available. Therefore, dual energy attenuation scaling would be restricted to the central part of the image. Further CT scanner development is required to broaden the dual energy field of view.

Dual source CT scanners are now commercially available and have a high clinical potential especially to improve cardiovascular CT imaging. The two x-ray tubes can be used to obtain a high temporal resolution by halving the gantry rotation angle necessary for image reconstruction and thereby reduce motion artifacts.[9] When used at different energies they can support differentiation of various materials and tissue types, e.g., bone and calcifications in vessel walls from intraluminal iodinated contrast media.[10,11]

Integration of dual source CT in PET/CT scanners could therefore be a further improvement of multimodality imaging notably of cardiovascular diseases. Moreover, the additional information provided by the two CT energies could be used to reduce beam hardening artifacts and linear attenuation coefficient transformation errors. The faster CT acquisition together with list mode PET acquisition should allow more precise heart imaging with movement corrected attenuation correction. However, the scan with two sources leads to increased noise in the attenuation correction factors (ACFs) and usually but not necessarily[12] increases the dose applied to the patient.

This work investigates the reduction of contrast agent linear attenuation coefficient transformation errors and the increased noise introduced by the two sources. The ambiguous map from linear attenuation coefficient at CT energy to PET energy is responsible for the error in the ACFs and makes further assumptions on the attenuating media necessary. The map is ambiguous, because the measured linear attenuation coefficient at CT energy does not fully specify the attenuating media and its constituents.[13] Usually bilinear or hybrid scaling methods[6,8,14] which assume human tissue as attenuating media are used. Materials of large atomic numbers like iodine (atomic number $Z=53$) do not fulfill this assumption and the mentioned scaling methods are therefore erroneous in the presence of CT contrast agents.[15–19]

Three different concepts of dual energy scaling are compared and discussed. In the two first concepts the attenuating media (the patient) is composed of one effective material at a given position. In the first concept the two energy scans are used to determine the probability of Compton and photoelectric effect.[12,20] Since the energy dependency of Compton and photoelectric effect are approximately known, the attenuation coefficient at PET energy can be extrapolated. The second approach is also motivated by physical properties. There the information of the two scans is used to determine the mean effective atomic number and electron density[21,22] which then can be used to obtain the attenuation coefficient at PET energy. The third method assumes that the media is a composition of two constituents and uses the information from the two energy scans to differentiate between two composition schemes (water-bone or water-iodine).[23,24]

II. THEORY

For PET and CT, the linear attenuation coefficient $\mu_{Z,A}$ of an element (Z,A) is the sum of Compton ($\mu^{\mathrm{C}}_{Z,A}$), photoelectric ($\mu^{\mathrm{P}}_{Z,A}$), and Rayleigh scattering components. Rayleigh scattering is unlikely at both, CT and PET energies. When Rayleigh scattering is neglected, the overall linear attenuation coefficient can be approximated by

$$\mu_{Z,A} = \mu^{\mathrm{C}}_{Z,A} + \mu^{\mathrm{P}}_{Z,A}. \tag{1}$$

The linear attenuation coefficient for the Compton effect μ^{C} is the product of the volume related electron density ρ^{e} of the material and the integral Klein–Nishina formula $K(E)$ at energy E

$$\mu^{\mathrm{C}}_{Z,A} = \rho^{\mathrm{e}}_{Z,A} K(E). \tag{2}$$

The photoelectric linear attenuation coefficient is approximately described by

$$\mu^{\mathrm{P}}_{Z,A} = kZ^m E^n A^{-1} \rho, \tag{3}$$

where k depends on the involved atomic shell, Z is the atomic number, A the atomic weight, and E and ρ are energy and density, respectively. The parameter m lies between 3 and 4 and n between -3 and -3.5.[12,25]

The overall linear attenuation coefficient μ_{eff} of a given material is the sum of the linear attenuation coefficients of its elements, weighted with the respective volume density $\alpha_{Z,A}$:

$$\mu_{\mathrm{eff}} = \sum_{Z,A} \alpha_{Z,A} \mu_{Z,A} = \sum_{Z,A} \alpha_{Z,A} (\mu^{\mathrm{C}}_{Z,A} + \mu^{\mathrm{P}}_{Z,A}). \tag{4}$$

The material would be fully specified and the transformation to PET energy straight forward, if the fractions $\{\alpha_{Z,A}\}_{Z,A}$ of all elements were known.

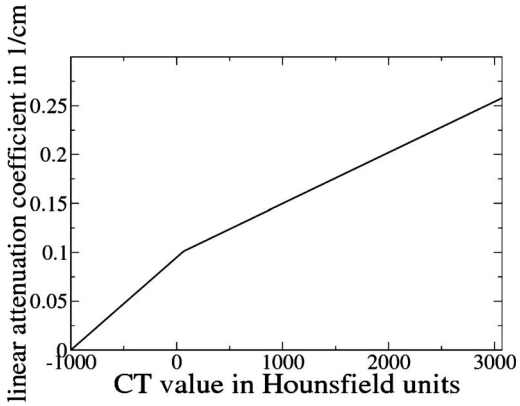

FIG. 1. Bilinear scaling from CT values at 140 kVp to linear attenuation coefficients at 511 keV as implemented at the Biograph 16 (see Ref. 14).

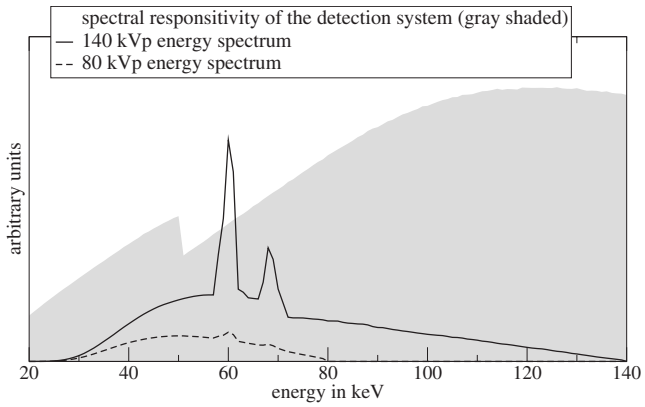

FIG. 2. CT energy spectra $S(E)$ of 140 and 80 kVp beams as well as the spectral responsitivity $D(E)$ of the detection system (see Ref. 30).

II.A. Single energy scaling

In commercially available PET/CT scanners a single CT scan is used to predict the linear attenuation of the material at PET energy (511 keV). The Biograph 16 uses bilinear scaling to transform the measured CT values to linear attenuation coefficient at 511 keV (see Fig. 1). Above a certain soft tissue CT value bone is assumed and the CT value is scaled accordingly.[14] This method was used in this work.

Other single energy scaling methods use trilinear scaling[26] or segment the CT images prior to scaling.[27] Thresholding methods were proposed to reduce contrast agent artifacts in single energy scaling.[28,29]

II.B. Compton/photoelectric effect - scaling

The Compton/photoelectric effect scaling method assumes that the material within the field of view can be described by effective linear attenuation coefficients for Compton and photoelectric effect. Equation (4) is therefore replaced by

$$\mu_{\mathrm{eff}}(E) \approx \mu_{\mathrm{eff}}^{\mathrm{C}}(E) + \mu_{\mathrm{eff}}^{\mathrm{P}}(E) \tag{5}$$

with

$$\mu_{\mathrm{eff}}^{\mathrm{C}}(E) = \rho_{\mathrm{eff}}^{\mathrm{e}} K(E) \tag{6}$$

$$\mu_{\mathrm{eff}}^{\mathrm{P}}(E) = a_{\mathrm{eff}} E^n, \tag{7}$$

where Eq. (6) is derived from Eq. (2) and a_{eff} is an effective parameter that does not depend on the photon energy (7). Effective energies $\breve{E}_i$ for 140 and 80 kVp can be calculated by evaluating

$$\breve{E}_i \equiv \int w_i(E) E \mathrm{d}E \tag{8}$$

with $w_i(E)$ being

$$w_i(E) \equiv \frac{S_i(E)D(E)}{\int S_i(E)D(E)\mathrm{d}E}. \tag{9}$$

Here $S(E)$ is the x-ray tube spectrum and $D(E)$ is the spectral responsitivity of the detection system (see Fig. 2). The spectral responsitivity $D(E)$ is the average light energy measured for an incoming x-ray quantum of energy E. We have $D(E) = \int (D(E,E')E'dE'$, where $D(E,E')$ is the detection probability density to measure an incoming x-ray photon of energy E as the light energy E' (see Ref. 30).

Equation (9) does not account for beam hardening.[31] The presented methods should therefore be applied to image data that are corrected for beam hardening. For two scans and by using Eqs. (5)–(7) this leads to two coupled equations

$$\mu_i^{\mathrm{eff}} \approx \rho_{\mathrm{eff}}^{\mathrm{e}} K(\breve{E}_i) + a_{\mathrm{eff}} \breve{E}_i^n \quad \text{for } i = 1,2 \tag{10}$$

with measured μ_i^{eff} and the unknowns $\rho_{\mathrm{eff}}^{\mathrm{e}}$ and a_{eff}. Two measurements at different peak energies are therefore sufficient to calculate the two unknowns. The obtained values can then be used in Eq. (5) to calculate the linear attenuation coefficient at E_{511}=511 keV for each pixel.[12]

$$\mu_{511} = \underbrace{\frac{\mu_1 \breve{E}_2^n - \mu_2 \breve{E}_1^n}{K(\breve{E}_1)\breve{E}_2^n - K(\breve{E}_2)\breve{E}_1^n}}_{\rho_{\mathrm{eff}}^{\mathrm{e}}} K(\breve{E}_{511}) + \underbrace{\frac{\mu_1 K(\breve{E}_2) - \mu_2 K(\breve{E}_1)}{K(\breve{E}_2)\breve{E}_1^n - K(\breve{E}_1)\breve{E}_2^n}}_{a_{\mathrm{eff}}} E_{511}^n. \tag{11}$$

We used $n=-3$ for our calculations. The effective energies $\breve{E}$ were 55.0 and 77.4 keV for 80 and 140 kVp, respectively.

II.C. (Z, ρ) - scaling

The linear attenuation coefficient is this time approximated by a material with effective atomic number Z_{eff}. For a polyenergetic beam with energy spectrum $S_i(E)$ the linear attenuation coefficient of a pixel becomes

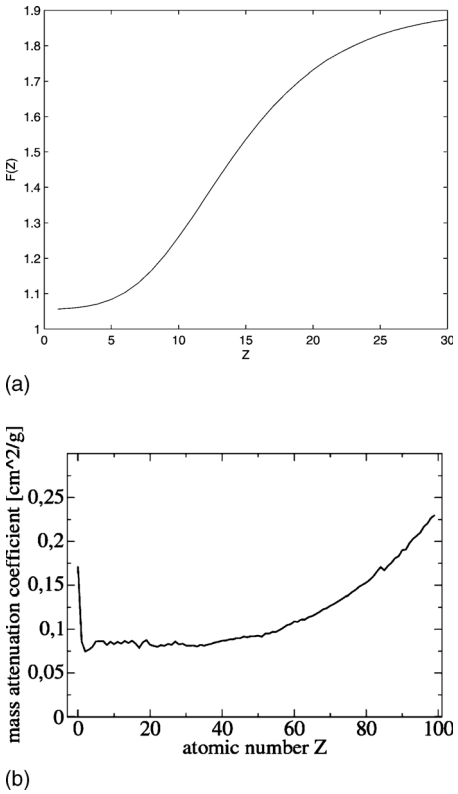

FIG. 3. (a) Function $F(Z)$ for 80 keV/140 keV dual energy scan with 1.2 mm titanium filter ("body") and (b) mass attenuation coefficient $\kappa(Z)=\mu/\rho$ at 511 keV for elements $Z=1$ to $Z=99$ (see Ref. 32).

$$\bar{\mu}_i(Z_{\text{eff}}) = \int w_i(E)\mu(Z_{\text{eff}},E)\mathrm{d}E. \tag{12}$$

Therefore, the ratio r between the linear attenuation coefficients $\bar{\mu}_i$ of two scans ($i=1,2$) can be calculated:

$$r \equiv \frac{\bar{\mu}_1(Z_{\text{eff}})}{\bar{\mu}_2(Z_{\text{eff}})} = \frac{\int w_1(E)\kappa(Z_{\text{eff}},E)\mathrm{d}E}{\int w_2(E)\kappa(Z_{\text{eff}},E)\mathrm{d}E} \equiv F(Z_{\text{eff}}). \tag{13}$$

The function $F(Z)$ can be determined by using mass attenuation coefficients $\kappa(Z,E)$ of experimental tables (i.e., Refs. 32–34) and by interpolating these tables for noninteger Z_{eff} values. $F(Z_{\text{eff}})$ is a monotone function [see Fig. 3(a) and Ref. 22] and can therefore be inverted.

$$Z_{\text{eff}} = F^{-1}(r), \quad \rho^{\text{e}}_{\text{eff}} = \frac{\mu_1}{\int w_1(E)\mu(F^{-1}(r),E)\mathrm{d}E}. \tag{14}$$

Given Z_{eff} and $\rho^{\text{e}}_{\text{eff}}$, the mass attenuation at 511 keV can be calculated by using again interpolated experimental mass attenuation tables [see Fig. 3(b)]. Multiplication with $\rho^{\text{e}}_{\text{eff}}$ yields the wanted linear attenuation coefficient.

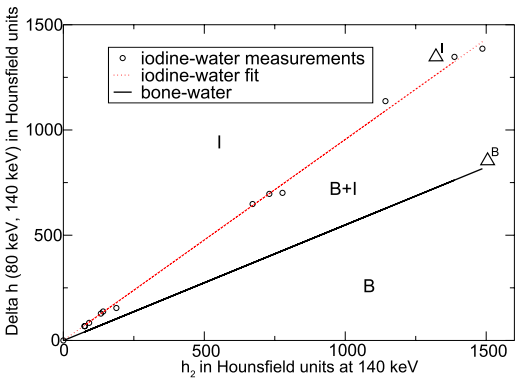

FIG. 4. Dependency of the difference of image values of iodine-water solutions for 140 and 80 kVp scans in Hounsfield units. The upper boundary (iodine-water) was obtained by fitting to CT measurements (circles) and the lower (bone-water) by using the default single energy bilinear scaling method (see Ref. 14).

II.D. Hybrid dual energy CT attenuation correction (hybrid DECTAC)

The hybrid dual energy CT attenuation correction scaling method uses the difference in Hounsfield units

$$\Delta h = h_1 - h_2 = h(E_1^{\text{P}}) - h(E_2^{\text{P}}) \tag{15}$$

between two scans at different peak energies E_1^{P} and E_2^{P} to classify the voxels into either a composition of water and bone (B), water and iodine (I), or a mixture of both (B+I). The two boundaries (see Fig. 4) can be determined by measurements of different iodine-water solutions [$\Delta^I(h_2)$ =upper boundary] and by the internal bilinear bone-water ACF scaling [$\Delta^B(h_2)$=lower boundary]. Given the two measured Hounsfield values Δh and h_2 of a pixel, this pixel is scaled by

$$\mu_{511} = (1-\alpha)F^{\text{B}}_{E_2^{\text{P}}\to 511}(h_2) + \alpha F^{\text{I}}_{E_2^{\text{P}}\to 511}(h_2) \tag{16}$$

with

$$\alpha = \max\left(\min\left(\frac{\Delta h - \Delta^{\text{B}}(h_2)}{\Delta^{\text{I}}(h_2) - \Delta^{\text{B}}(h_2)}, 1\right), 0\right) \tag{17}$$

and

$$F^{\text{B}}_{E_2^{\text{P}}\to 511}(h_2) \quad \text{and} \quad F^{\text{I}}_{E_2^{\text{P}}\to 511}(h_2) \tag{18}$$

being the bilinear scaling for bone-water and iodine-water compositions from Hounsfield units h_2 to linear attenuation coefficients at energy $E_{511}=511$ keV. We used dual energy scans with $E_1^{\text{P}}=80$ kVp and $E_2^{\text{P}}=140$ kVp.

The implemented hybrid DECTAC scaling method is a variant of the hybrid DECTAC scaling method presented by Kinahan *et al.*[24] with an additional interpolated region B+I between the region B and region I (see Fig. 4).

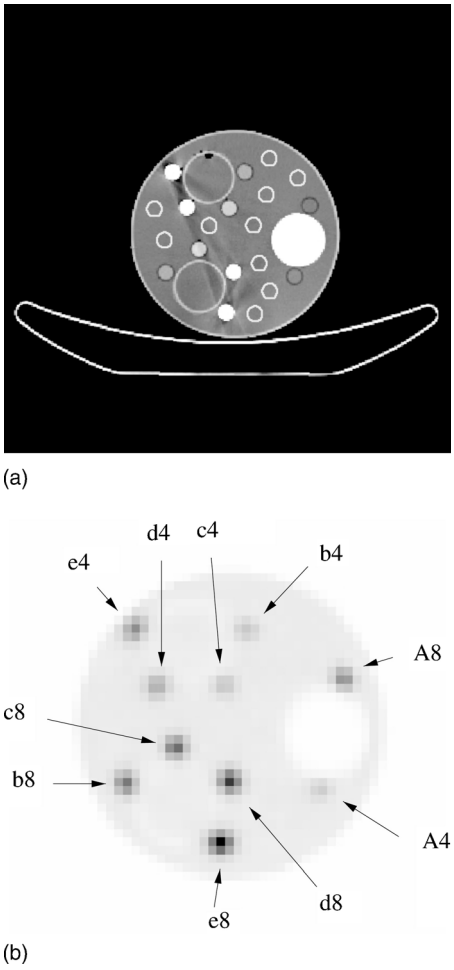

FIG. 5. CT and PET image of a central slice of the phantom. (a) CT scan at 120 kVp and effective 160 mAs. The empty white circles show the position of the background ROIs used for NEMA-like percent contrast evaluation. (b) PET reconstruction using a CT scan at 80 kVp and effective 160 mAs.

III. METHODS

III.A. Phantom

Measurements were performed with a modified National Electric Manufacturers Association (NEMA) 1994 PET phantom using the Biograph 16-HIREZ, a lutetium oxyorthosilicate (LSO) based PET/CT scanner with Pico3D electronics (Siemens Medical Solutions, USA). The two fillable inserts as well as the rest of the phantom were filled with 11 kBq/ml [^{18}F] fluorodeoxyglucose ([^{18}F]FDG) background concentration. Plastic Falcon tubes (inner diameter 15 mm, around 18 ml) with different contrast agent and FDG ratios were inserted into the phantom and attached to the fillable inserts as well as to the Teflon insert by small cable binders. Five different contrast agent concentrations c=0%, 1%, 2%, 10%, and 20% Imeron 400-water solutions (Imeron 400: Bracco ALTANA pharma GmbH, Germany; 400 mg iodine/ml) and two different FDG concentrations (4× and 8× the background emission density) were used in the tubes (see Fig. 5 and Table I).

TABLE I. Labels used in Fig. 5(b).

Label	c	[^{18}F]FDG
A8	0	8:1
b8	1%	8:1
c8	2%	8:1
d8	10%	8:1
e8	20%	8:1
A4	0	4:1
b4	1%	4:1
c4	2%	4:1
d4	10%	4:1
e4	20%	4:1

III.B. Measurement

After the acquisition of the CT topogram, six CT image sets covering the same field of view (FOV) were acquired. Four measurements with effective tube current time products of 160 mAs at energies of 140, 120, 100, and 80 keV were performed. In addition, two measurements with 30 mAs at energies of 140 and 80 keV were performed in order to investigate the influence of CT noise. After these CT scans one PET scan at a single bed position was acquired in a 30 min measurement.

III.C. Scaling of the linear attenuation coefficients

Single energy scaling used the default scaling method.[14] The dual energy scaling methods used the algorithms that are described in Sec. II to predict the linear attenuation coefficient μ at 511 keV. Then, these coefficients μ were transformed by the inverse of the default scaling method to Hounsfield units at 140 kVp. These artificial 140 kVp CT images were then fed into the built-in reconstruction program. In this way the same reconstruction software and parameters were used and the methods could be directly compared.

III.D. PET image reconstruction

PET images were reconstructed using attenuation weighted ordered subset expectation maximization using four iterations with eight subsets and model based scatter correction.[35] Images were post smoothed with a 5 mm three-dimensional Gaussian Kernel. Image size was 128×128 pixels with a voxel size of 5.33 mm×5.33 mm and slice thick-

TABLE II. Linear attenuation coefficients μ in 1/cm for water and Teflon at 511 keV using different scaling methods.

Method	Water	Teflon
True	0.095	0.182
Single energy scaling (140 kVp)	≈0.095	≈0.145
Single energy scaling (80 kVp)	≈0.095	≈0.141
Compton effect/photoelectric effect	≈0.097	≈0.178
(Z,ρ) scaling	≈0.086	≈0.158
hybrid DECTAC	≈0.095	≈0.145

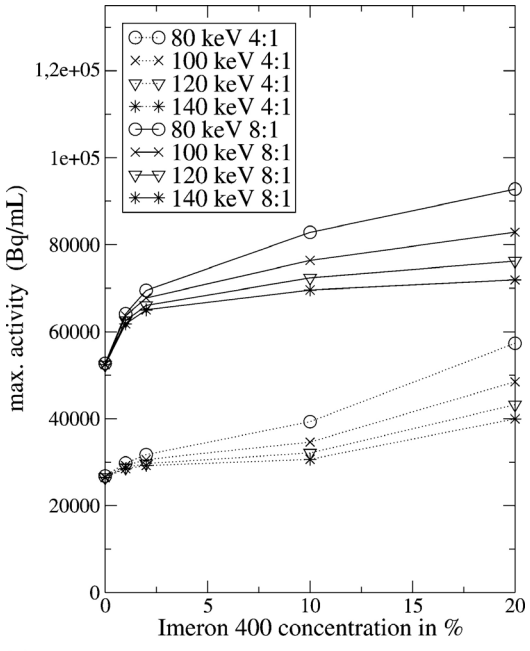

FIG. 6. The influence of CT energy and contrast agent concentration on the reconstructed emission density. Twenty percent Imeron 400 concentration corresponds to 80 mg iodine/ml. See Fig. 5 for the positioning of the falcon tubes with different contrast-agent solutions. (a) Graph showing the concentration dependency and CT energy dependency of the maximal ROI value. (b) Graph showing the concentration dependency and CT energy dependency of percent contrast.

ness of 2 mm. In six separate reconstructions each of the CT scans was used for attenuation correction. In addition, 140 and 80 kVp scans were used for dual energy attenuation correction.

TABLE III. Maximal ROI value [kBq/ml] of the falcon tubes with 4:1 activity ratio and Imeron 400 iodine constrast agent concentrations 0%, 1%, 2%, 10%, and 20%.

	0%	1%	2%	10%	20%
Single energy 140 keV	26.5	28.5	29.2	30.7	40.0
Compton/photoelectric	31.0	30.6	31.0	31.4	37.3
(Z,ρ)	20.1	17.6	21.2	22.6	22.7
Hybrid DECTAC	25.8	26.4	26.1	24.0	27.5

IV. EVALUATION

IV.A. Scaled linear attenuation coefficient μ for water and Teflon

The proposed dual energy scaling methods should correctly extrapolate the linear attenuation coefficient of water. It is desirable that the methods are robust, i.e., also work correctly for materials not included into the scaling scheme (for example, Teflon as opposed to water, bone, or iodine for hybrid DECTAC). Therefore, the mean predicted linear attenuation coefficients of water and Teflon were determined by evaluating two 15-mm-diameter circular regions of interest (ROIs) in the scaled μ images that were placed in the water and Teflon regions, respectively.

IV.B. Maximal voxel value and percent contrast of PET images

The PET images were evaluated by circular ROIs covering the 15-mm-diam falcon tubes in transversal images. Largest pixel values as well as percent contrast were determined. The mean background activity that is needed for percent contrast evaluation was calculated by averaging over ten background regions of interest (bROIs) of the same size. These regions were placed in the background of the evaluated slice [see Fig. 5(a)] and ± 1 and ± 2 cm axially displaced slices, therefore forming a set of 50 bROI. Percent contrast Q is calculated as in the NEMA NU2-2001 standard:

$$Q = \frac{\dfrac{\text{mean ROI value}}{\text{mean bROI value}} - 1}{\text{true activity ratio} - 1} \times 100\,\% \,. \tag{19}$$

TABLE IV. PET percent contrast Q of the falcon tubes with 4:1 activity ratio and Imeron 400 iodine constrast agent concentrations 0%, 1%, 2%, 10%, and 20%.

	0%	1%	2%	10%	20%
Single energy 140 keV	22.6%	28.5%	31.3%	40.0%	48.3%
Compton/photoelectric	28.5%	27.5%	27.5%	33.6%	38.1%
(Z,ρ)	27.3%	27.4%	22.9%	18.4%	21.4%
Hybrid DECTAC	24.2%	27.6%	26.2%	26.9%	29.2%

IV.C. Noise in (artificial) CT images and background variability in the PET images

The influence of the effective CT current time product on the noise in the CT images (single energy scaling) and artificial CT images (dual energy scaling) was evaluated by the standard deviation (SD) of the voxels inside a circular ROI with 15 mm diameter placed in the background of the phantom.

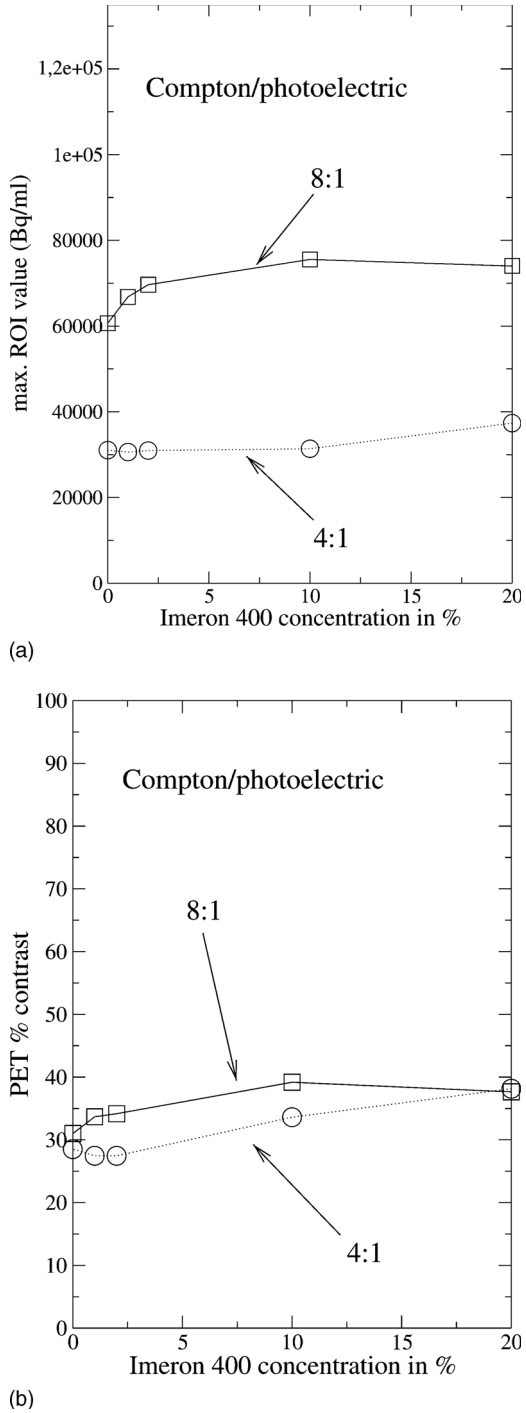

FIG. 7. The influence of contrast agent concentration on the reconstructed emission density with Compton/photoelectric effect dual energy attenuation correction (see Fig. 5). (a) Maximal ROI value (b) percent contrast.

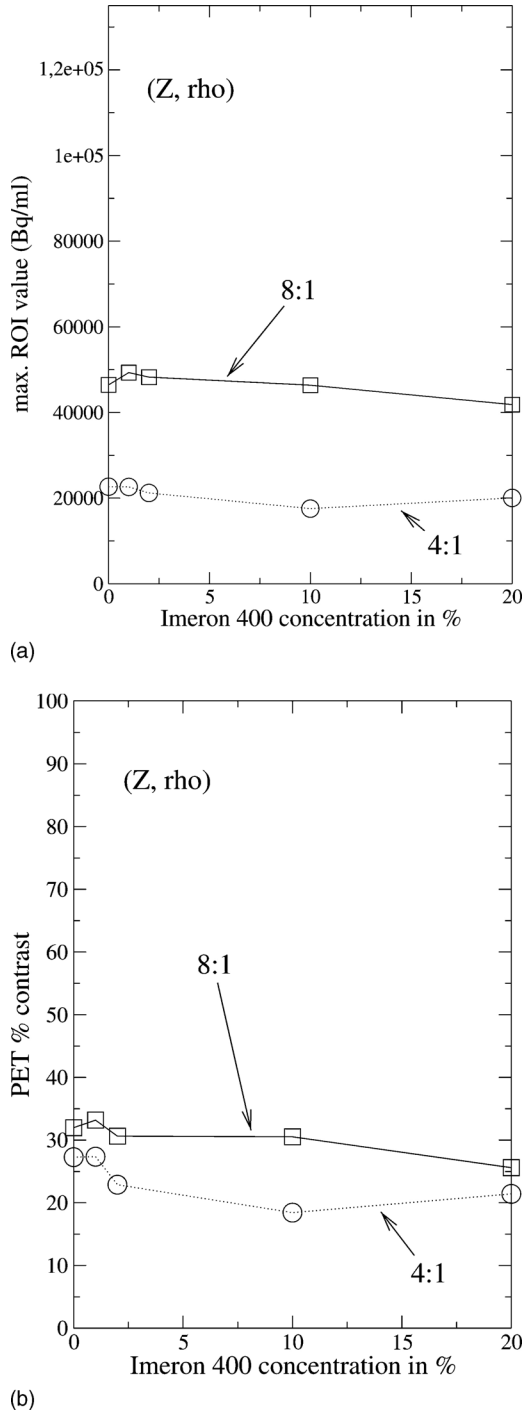

FIG. 8. The influence of contrast agent concentration on the reconstructed emission density with (Z,ρ) dual energy attenuation correction (see Fig. 5). (a) Maximal ROI value (b) percent contrast.

Finally, background variability of the PET images was calculated similarly to NEMA NU2-2001 standard using the 50 bROI specified in Sec. IV B:

$$N = \frac{\text{standard deviation of 50 bROI values}}{\text{mean of 50 bROI values}} \times 100\,\% \,. \tag{20}$$

V. RESULTS

V.A. Scaled linear attenuation coefficient μ for water and Teflon

Table II shows the calculated linear attenuation coefficients based on the CT measurements for water and Teflon at 511 keV using the different scaling methods. Single energy scaling and hybrid DECTAC work best to estimate the true linear attenuation coefficient $\mu=0.095\ \mathrm{cm}^{-1}$ for water. Compton/photoelectric effect as well as (Z,ρ) scaling leads to a stronger deviation by either overestimating ($0.097\ \mathrm{cm}^{-1}$) or underestimating ($0.086\ \mathrm{cm}^{-1}$) the linear attenuation coefficient.

In contrast, for Teflon ($\mu=0.182\ \mathrm{cm}^{-1}$), Compton/photoelectric effect scaling works best ($0.178\ \mathrm{cm}^{-1}$) followed by (Z,ρ) scaling ($0.158\ \mathrm{cm}^{-1}$). Single energy scaling or hybrid DECTAC strongly underestimate the linear attenuation coefficient with values between 0.141 and $0.145\ \mathrm{cm}^{-1}$.

V.B. Maximal voxel value and percent contrast of PET images

The influence of the contrast agent concentration as well as the CT peak energy on the reconstructed activity using bilinear scaling is shown in Fig. 6(a) (maximal ROI value) and Fig. 6(b) (percent contrast). The corresponding values for the falcon tubes with 4:1 activity ratio can be seen in Tables III and IV, respectively. Clearly, an increase in the concentration or a decrease of the CT peak energy leads to higher values as expected. The best performance could be achieved with 140 keV CT images.

In Figs. 7–9 the influence of the contrast agent concentration on the maximal ROI value (a) as well as on percent contrast (b) for dual energy scaling methods can be seen. All methods clearly counterbalance to some extent the undesirable trend of larger values for regions with higher concentration. Tables III and IV show the maximal ROI values and PET percent contrast for the 4:1 activity ratio falcon tubes.

V.C. Noise in (artificial) CT images and background variability in the PET images

The standard deviation (SD) of voxels of the CT images and the background variability (N) of the PET images are shown in Table V. For single CT scans (first four rows in Table V) the standard deviation increases strongly (approximately 3×) if the mean current time product is reduced from 160 to 30 mAs, but also when 80 kVp is used instead of 140 kVp (approximately 2×). The first observation also applies for the artificial CT images obtained by the dual energy scaling methods.

The use of 80 keV CT images in single energy attenuation correction results in increased background variability in comparison to 140 keV images (3.4% versus 2.6%–2.7%). The effective current time product has very little (2.6% versus 2.7%) or no impact (3.4% versus 3.4%). The background variability for Compton/photoelectric effect scaling or hybrid DECTAC is even lower (2.1%) than the background variability of PET images that were scaled bilinearly with 140 keV and 160 mAs (2.6%). The reduction of the current time product had no effect for these two dual energy scaling methods. (Z,ρ) scaling with N values of 4.3% and 4.9% showed the worst performance and also showed a dependency on the current time product.

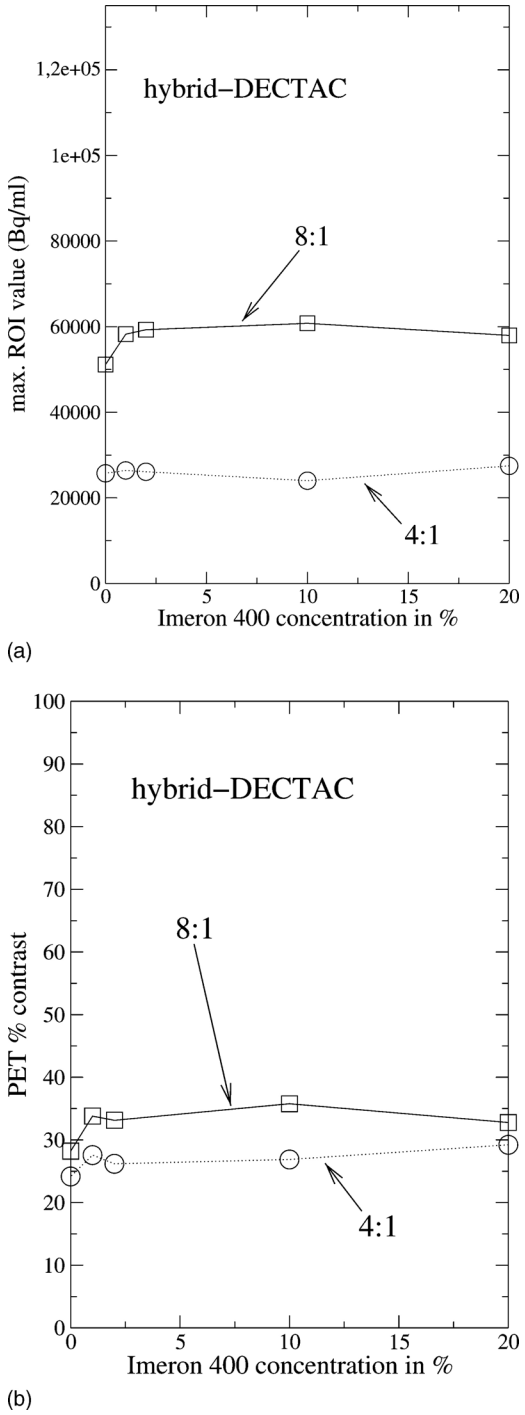

FIG. 9. The influence of contrast agent concentration on the reconstructed emission density with hybrid DECTAC (see Fig. 5). (a) Maximal ROI value (b) percent contrast.

VI. DISCUSSION

Due to the still incomplete information about the material composition of the scanned patient/phantom, all three dual

TABLE V. Standard deviation (SD) of the pixel values of a circular ROI with 15 mm diameter that is placed in the water background of the (artificial) CT and percent background variability (N) of the PET image for different scaling methods.

Method	140 kVp	80 kVp	SD	N
Single energy	160 mAs	···	3.6	2.6%
Single energy	30 mAs	···	9.3	2.7%
Single energy	···	160 mAs	8.7	3.4%
Single energy	···	30 mAs	19.2	3.4%
Compton/photoelectric	160 mAs	160 mAs[a]	7.3	2.1%
Compton/photoelectric	30 mAs	30 mAs[a]	20.0	2.1%
(Z,ρ) scaling	160 mAs	160 mAs[a]	12.2	4.3%
(Z,ρ) scaling	30 mAs	30 mAs[a]	30.0	4.9%
hybrid DECTAC	160 mAs	160 mAs[a]	3.3	2.1%
hybrid DECTAC	30 mAs	30 mAs[a]	8.0	2.1%

[a]Due to inexact repositioning 80 kVp images were shifted by half a CT slice versus 140 kVp images. Therefore, 80 kVp images were linearly interpolated before dual energy correction in order to obtain the same position.

energy scaling methods and of course also the single energy scaling method are only correct for a subset of all possible materials.

In single energy scaling, the coefficients for Teflon are underestimated, because it is classified as "bone." This applies also to hybrid DECTAC. Teflon is a mixture of atoms with lower mean atomic number ($Z_{\text{eff}}=8.3$) than bone (cortical bone: $Z_{\text{eff}}=10.9$).[36] The photoelectric effect is less important in Teflon than it is in bone and the single energy scaling therefore overcorrects (and therefore underestimates) the linear attenuation coefficients of Teflon at higher energies. On the other hand, the linear attenuation coefficient of iodine is strongly overestimated.

The Compton/photoelectric effect scaling performs quite well in terms of the linear attenuation coefficient of Teflon (compared to the other methods), but overestimates the linear attenuation coefficient for water. The maximum voxel values for the contrast agent-free falcon tubes (either 4:1 or 8:1) are higher than in the images that are attenuation corrected with single energy scaling (31.0 kBq/ml versus 26.5 kBq/ml for the 4:1 tubes). This indicates also that water scaling is problematic. The percent contrast plot and maximum voxel plot show that the linear attenuation coefficients for iodine-water solutions are only weakly overestimated.

The disability of the (Z,ρ) scaling method to correctly scale water can be explained by Fig. 3(b). While predicting relative correctly the effective atomic number $Z_{\text{eff}}=7.3$ for water, the calculation of 511 keV linear attenuation coefficient through Fig. 3(b) does not account for the abnormal behavior of hydrogen. By using a $\mu(Z)$ value between $Z=7$ (nitrogen, $\mu=0.0864$) and $Z=8$ (oxygen, $\mu,=0.0865$) the linear attenuation of water (including hydrogen) is therefore underestimated (see Table II). This also implies that other material compositions that include hydrogen are wrongly treated. Maximum voxel and percent contrast plots show no positive trend for higher iodine-water solutions.

The water scaling problem does not arise for hybrid DECTAC, because here water is classified correctly as water and the respective scaling is applied. Despite the correctly scaled water, percent contrast is slightly higher for the falcon tubes without contrast agent in the hybrid DECTAC scaled images (24.2%) than in the single energy scaled images (22.6%). Since both methods scale water (and Teflon) in the same manner (see Table II), the increase must be caused by beam hardening artifacts in the background ROIs used for percent contrast calculation. This explanation is also supported by reduced PET background variability N and comparable maximal ROI voxel values of 26.6% kBq/ml and 25.8% kBq/ml for the 4:1 falcon tubes of single energy 140 keV and hybrid DECTAC scaled images, respectively.

It can be expected that noise in the artificial CT (SD) as well as PET (N) images should be increased when dual energy scaling methods are used. Despite the (Z,ρ) scaling scheme this could not be verified. For the two other methods background variability was even decreased and, in addition, the hybrid DECTAC method also resulted in smaller SD values.

The repeated CT measurements with different kVp and mAs values required the movement of the CT table and the acquired images were half a slice offset for different settings and therefore two neighboring 80 kVp images were used to interpolate an image that is positioned at the same position as the 140 kVp image. Therefore, dual energy attenuation correction as implemented here used in principle three image slices to perform the scaling. This could explain the slightly better performance of hybrid DECTAC in contrast to 140 kVp single energy scaling. The lower background variability in the PET images, however, is probably caused by weaker beam hardening artifacts in the artificial CT images used for scaling.

Generally, the activity in the falcon tubes with no contrast agent in contrast to the other falcon tubes could be slightly underestimated due to the arrangement of the tubes. Due to space limitations and in contrast to the other falcon tubes, these tubes were attached to the Teflon insert which contained no activity (see Fig. 5). It can be expected that the large cold Teflon spot slightly biases the activity in the attached tubes toward lower activity. This effects all Figs. 6–9. It can therefore be assumed that hybrid DECTAC and Compton/photoelectric effect scaling that could reduce the

increase of PET percent contrast due to 20% Imeron 400 solution to only 5–10 percentage points (24.2% → 29.2% and 28.5% → 38.1%, respectively), perform even better than that.

Among the three presented dual energy scaling methods the hybrid DECTAC method is best suited for the usage together with CT contrast agents, but it can fail for other materials than water, iodine or bone. Future methods based upon this scheme should therefore classify more tissue/material types for the given information of $(h, \Delta h)$. A similar improvement can be envisaged also for the (Z, ρ) method, if Z_{eff} was used not to define the mass attenuation coefficient of an interpolated element Z [see Fig. 3(b)] but to determine the most likely tissue/material composition and use the respective mass attenuation coefficient. This could be, done, for example, by modifying Fig. 3(b) accordingly. The Compton/photoelectric effect scaling, although physically most appealing, lacks this ability to handle material compositions (including especially hydrogen).

Finally, it should be remarked that further improvement can be anticipated from iterative dual energy CT image calculations, especially with respect to reduced beam hardening artifacts.

VII. CONCLUSIONS

Three scaling methods for the linear attenuation coefficients based upon two CT scans of different energies were introduced, tested by applying them to experimental data, evaluated, and discussed. Among them hybrid DECTAC achieved the best results in terms of accuracy, noise, and extensibility. The other two methods, Compton/photoelectric effect and (Z, ρ) scaling, have problems with scaling water, although the latter could be extended to perform better for water and other materials. CT noise was not problematic except for (Z, ρ) scaling that was affected and resulted in increased background variability. (Z, ρ) scaling and hybrid DECTAC have the potential to be extended to perform better for larger number of materials.

Dual energy scaling methods, preferably hybrid DECTAC, should be used whenever two CT scans at different kVp but the same position and time are available, because dual energy scaling methods can outperform single energy scaling in the presence of iodine based contrast agents. Hybrid DECTAC can be understood as a generalization of the single energy scaling with the same advantages and fewer disadvantages.

ACKNOWLEDGMENTS

The authors would like to thank C. Michel, V. Rappoport, S. Käpplinger, and F. Schoenahl from Siemens Medical Solutions for their support and helpful discussions.

[a]Author to whom correspondence should be addressed; Electronic mail: niklasr@gmx.de

[1]D. W. Townsend, J. P. J. Carney, J. T. Yap, and N. C. Hall, "PET/CT today and tomorrow," J. Nucl. Med. **45**(1(Suppl)), 4S–14S (2004).
[2]A. C. Pfannenberg, P. Aschoff, K. Brechtel, M. Müller, M. Klein, R. Bares, C. D. Claussen, and S. M. Eschmann, "Value of contrast-enhanced multiphase CT in combined PET/CT protocols for oncological imaging," Br. J. Radiol. **80**(954) 437–445 (2007).
[3]P. E. Kinahan, D. W. Townsend, T. Beyer, and D. Sashin, "Attenuation correction for a combined 3D PET/CT scanner," Med. Phys. **25**(10), 2046–2053 (1998).
[4]Y. Nakamoto, M. Osman, C. Cohade, L. T. Marshall, J. M. Links, S. Kohlmyer, and R. L. Wahl, "PET/CT: Comparison of quantitative tracer uptake between germanium and CT transmission attenuation-corrected images," J. Nucl. Med. **43**(9), 1137–1143 (2002).
[5]C. Burger, G. Goerres, S. Schoenes, A. Buck, A. H. R. Lonn, and G. K. Schulthess, "PET attenuation coefficients from CT images: Experimental evaluation of the transformation of CT into PET 511-keV, attenuation coefficients," Eur. J. Nucl. Med. **29**(7), 922–926 (2002).
[6]P. E. Kinahan, B. H. Hasegawa, and T. Beyer, "X-ray-based attenuation correction for positron emission tomography/computed tomography scanners," Semin Nucl. Med. **XXXIII**(3), 166–179 (2003).
[7]H. Zaidi and B. Hasegawa, "Determination of the attenuation map in emission tomography," J. Nucl. Med. **44**, 291–315 (2003).
[8]C. C. Watson, V. Rappoport, D. Faul, D. W. Townsend, and J. P. Carney, "A method for calibrating the CT-based attenuation correction of PET in human tissue," IEEE Trans. Nucl. Sci. **53**(1), 102–107 (2006).
[9]A. J. Reimann, D. Rinck, A. Birinci-Aydogan, M. Scheuering, C. Burgstahler, S. Schroeder, H. Brodoefel, I. Tsiflikas, T. Herberts, T. Flohr, T. C. D. Claussen, A. F. Kopp, and M. Heuschmid, "Dual-source computed tomography: Advances of improved temporal resolution in coronary plaque imaging," Invest. Radiol. **42**(3), 196–203 (2007).
[10]T. R. Johnson, B. Krauss, M. Sedlmair, M. Grasruck, H. Bruder, D. Morhard, C. Fink, S. Weckbach, M. Lenhard, B. Schmidt, T. Flohr, M. F. Reiser, and C. R. Becker, "Material differentiation by dual energy CT: Initial experience," Eur. Radiol. **17**(6), 1510–1517 (2007).
[11]D. T. Boll, M. H. Hoffmann, N. Huber, A. S. Bossert, A. J. Aschoff, and T. R. Fleiter, "Spectral coronary multidetector computed tomography angiography: Dual benefit by facilitating plaque characterization and enhancing lumen depiction," J. Comput. Assist. Tomogr. **30**(5), 804–811 (2006).
[12]M. J. Guy, I. A. Castellano-Smith, M. A. Flower, G. D. Flux, R. J. Ott, and D. Visvikis, "DETECT—dual energy transmission estimation CT—for improved attenuation correction in SPECT and PET," IEEE Trans. Nucl. Sci. **45**(3), 1261–1267 (1998).
[13]W. Schneider, T. Bortfeld, and W. Schlegel, "Correlation between CT numbers and tissue parameters needed for Monte Carlo simulations of clinical dose distributions," Phys. Med. Biol. **45**, 459–478 (2000).
[14]J. P. J. Carney, D. W. Townsend, V. Rappoport, and B. Bendriem, "Method for transforming CT images for attenuation correction in PET/CT imaging," Med. Phys. **33**(4), 976–983 (2006).
[15]G. Antoch, L. S. Freudenberg, T. Engelhof, J. Stattaus, W. Jentzen, J. F. Debatin, and A. Bockisch, "Focal tracer uptake: A potential artifact in contrast-enhanced dual-modality PET/CT scans," J. Nucl. Med. **43**(10), 1339–1342 (2002).
[16]Y.-Y. Yau, W.-S. Chan, Y.-M. Tam, P. Vernon, S. Wong, M. Coel, and S. Kwok-Fai Chu, "Application of intravenous contrast in PET/CT: Does it really introduce significant attenuation correction error?" J. Nucl. Med. **46**(2), 283–291 (2002).
[17]Y. Nakamoto, B. B. Chin, D. L. Kraitchman, L. P. Lawler, L. T. Marshall, and R. L. Wahl, "Effects of nonionic intraveneous contrast agents at PET/CT imaging: Phantom and canine studies," Radiology **227**, 817–824 (2003).
[18]G. Antoch, L. S. Freudenberg, T. Beyer, A. Bockisch, and J. F. Debatin, "To enhance or not to enhance? ^{18}F-FDG and CT contrast agents in dual-modality ^{18}F-FDG PET/CT," J. Nucl. Med. **45**(1), 56S–61S (2004).
[19]O. Mawlawi, J. J. Erasmus, R. F. Munden, T. Pan, A. E. Knight, H. A. Macapinlac, D. A. Podoloff, and M. Chasen, "Quantifying the effect of IV contrast media on integrated PET/CT: Clinical evaluation," AJR, Am. J. Roentgenol. **186**, 308–319 (2006).
[20]R. E. Alvarez and A. Macovski, "Energy-selective reconstruction in x-ray computerized tomography," Phys. Med. Biol. **21**(5), 733–744 (1976).
[21]G. Christ, "Exact treatment of the dual-energy method in CT using polyenergetic x-ray spectra," Phys. Med. Biol. **29**(12), 1501–1510 (1984).
[22]B. J. Heismann, J. Leppert, and K. Stierstorfer, "Density and atomic number measurements with spectral x-ray attenuation method," J. Appl. Phys. **94**(3), 2073–2079 (2003).
[23]P. E. Kinahan, J. A. Fessler, A. M. Alessio, and T. K. Lewellen, "Quantitative attenuation correction for PET/CT using iterative reconstruction

of low-dose dual-energy CT," *Nuclear Science Symposium/Medical Imaging Conference Record*, pp. 3285–3289 (2004).
[24]P. E. Kinahan, A. M. Alessio, and J. A. Fessler, "Dual energy CT attenuation correction methods for quantitative assessment of response to cancer therapy with PET/CT imaging," Technol. Cancer Res. Treat. **5**(4), 319–327 (2006).
[25]Z. H. Cho, C. M. Tsai, and G. Wilson, "Study of contrast and modulation mechanisms in x-ray/photon transverse axial transmission tomography," Phys. Med. Biol. **20**(6), 879–889 (1975).
[26]M. Abella, D. Mankof, J. J. Vaquero, M. Desco, and P. E. Kinahan, "Accuracy of CT-based attenuation correction in bone imaging with PET/CT," *IEEE Nuclear Science Symposium Conference Record*, pp. 4485–4488 (2007).
[27]C. Bai, C.-H. Tung, J. Kolthammer, L. Shao, K. M. Brown, Z. Zhao, A. J. Da Silva, J. Ye, D. Gagnon, M. Parma, and E. Walsh, "CT-based attenuation correction in PET image reconstruction for the Gemini system," *Nuclear Science Symposium Conference Record*, Vol. 5, pp. 3082–3086 (2004).
[28]J. Carney, T. Beyer, D. Brasse, J. T. Yap, and D. W. Townsend, "CT-based attenuation correction for PET/CT scanners in the presence of contrast agent," *Nuclear Science Symposium Conference Record*, Vol. 3, pp. 1443–1446 (2002).
[29]F. Büther, L. Stegger, M. Dawood, F. Range, M. Schäfers, R. Fischbach, T. Wichter, O. Schober, and, K. P. Schäfers, "Effective methods to correct contrast agent-induced errors in PET quantification in cardiac PET/CT," J. Nucl. Med. **48**(7), 1060–1068 (2007).
[30]S. Wirth, W. Metzger, K. Pham-Gia, and B. J. Heismann, "Impact of photon transport properties on the detection efficiency of scintillator arrays," *IEEE Nuclear Science Symposium Conference Record*, pp. 2602–2603 (2006).
[31]R. A. Brooks and G. Di Chiro, "Beam hardening in x-ray reconstructive tomography," Phys. Med. Biol. **21**, 390–398 (1976).
[32]National Institute of Standards and Technology NIST, X-COM: Photon cross sections database.
[33]S. T. Perkins, D. E. Cullen, M. H. Chen, J. H. Hubbell, J. Rathkopf, and J. Scofield, "Tables and graphs of atomic subshell and relaxation data derived from the LLNL evaluated atomic data library (EADL)," Technical report, Lawrence Livermore National Laboratory, 1991.
[34]D. E. Cullen, M. H. Chen, J. H. Hubbell, S. T. Perkins, E. F. Plechaty, J. A. Rathkopf, and J. H. Scofield, "Tables and graphs of photon-interaction cross sections from 10 eV to 100 GeV, derived from the LLNL evaluated photon data library (EPDL)," Technical report, Lawrence Livermore National Laboratory, 1989.
[35]C. C. Watson, "New, faster, image-based scatter correction for 3D PET," IEEE Trans. Nucl. Sci. **47**(4), 1587–1594 (2000).
[36]International Commission on Radiation Units and Measurements (ICRU). Report No. 44, Tissue Substitutes in Radiation Dosimetry and Measurement, ICRU, 1989.